Journal of Translational Medicine

RESEARCH

Open Access

Dissecting the immunosuppressive microenvironment of LAMA3 + malignant cells and SPP1 + macrophages in esophageal squamous cell carcinoma using single-cell and spatial transcriptomics

Kunqiao Hong[1,2†], Chengzhou Pa[3†], Yijie Zhu[1], Yunrui Dai[4], Jialong Qi[2,5*] and Ping Wan[1,2*]

Abstract

Background Esophageal squamous cell carcinoma (ESCC) exhibits pronounced tumor microenvironment (TME) heterogeneity, which contributes to tumor invasion, immune evasion, and resistance to therapy. However, the cellular and spatial mechanisms driving this heterogeneity remain incompletely understood.

Methods We integrated single-cell RNA sequencing and spatial transcriptomics to characterize the cellular composition, spatial organization, and tumor–immune interactions within ESCC tissues. Ligand–receptor communication was inferred using NicheNet modeling, and functional roles of key genes were evaluated through in vitro assays.

Results We identified a LAMA3⁺ epithelial subpopulation enriched at the invasive tumor front, characterized by strong epithelial–mesenchymal transition (EMT) signatures and poor prognostic relevance. Tumor-enriched SPP1⁺ macrophages with M2-like phenotypes were also identified and associated with adverse clinical outcomes. Spatial analyses revealed close colocalization of LAMA3⁺ epithelial cells and SPP1⁺ macrophages, while NicheNet modeling indicated reciprocal ligand–receptor interactions that directly mediated the extracellular matrix, and promoted desmoplastic niche formation. This cooperative network restricted lymphocyte infiltration despite a high tumor mutational burden, leading to an immune-excluded microenvironment. Clinically, co-enrichment of *LAMA3* and *SPP1* predicted impaired responses to anti–PD-L1 therapy. Functional assays further confirmed that LAMA3 promotes tumor cell proliferation, migration, and invasion.

†Kunqiao Hong and Chengzhou Pa contributed equally to this work.

*Correspondence:
Jialong Qi
962992598@qq.com
Ping Wan
sqxn2kkkq@126.com

Full list of author information is available at the end of the article

Conclusions Our study identifies a synergistic LAMA3–SPP1 axis that promotes desmoplastic remodeling and immune evasion in ESCC, suggesting a potential therapeutic target to improve immunotherapy outcomes.

Materials and methods

The scRNA seq data clustering, dimension reduction and cell annotation

Single-cell data analysis was performed using the "Seurat" package. Data integration across samples was conducted using the "Harmony" algorithm. Single-cell gene expression data of all patients were merged, and transcriptomes were filtered for cells with 500–10,000 genes detected, 1000–100,000 UMIs counted, fraction of mitochondrial reads < 15%. After filtering, Gene expression values were scaled with "ScaleData", and principal component analysis (PCA) was conducted on variable genes using "RunPCA". The first 20 principal components were utilized for clustering via "FindNeighbors" and "FindClusters" (resolution = 0.5). UMAP was applied to the top 30 principal components for dimensionality reduction and visualization. Marker genes for each clusters were determined using "FindAllMarkers", with thresholds set at log fold change > 0.5, minimum expression fraction (min.pct) > 0.25, and adjusted p-value < 0.05.

Estimation of the activity of diverse signatures and pathways

The "GSVA" algorithm was applied to assess the relative activation status of specific gene signatures or pathways. GSVA scores were calculated for cancer hallmark signatures and key signaling pathways using predefined gene sets obtained from the Molecular Signatures Database (MSigDB).

Cellular communication analysis

CellCall analysis was performed to infer intercellular communication networks and identify potential signaling interactions. Using the "CellCall" package, we processed the single-cell RNA-seq data to predict ligand-receptor interactions between different cell types. This approach enables the identification of key signaling pathways involved in cellular communication within the tumor microenvironment, contributing to the understanding of immune modulation and tumor progression.

CNV analysis

Somatic copy number variations (CNVs) were inferred using InferCNV (v0.8.2, https://github.com/broadinstitute/infercnv), with adjacent normal epithelial cells serving as the reference [1]. In brief, gene-level expression data were mapped to their corresponding chromosomal locations, and genes lacking chromosomal annotations were excluded. CNV profiles were then calculated for each cell, and cells were classified as putative malignant if they had a CNV score > 0.05 and CNV correlation > 0.5. To explore CNV patterns, cells were clustered based on their CNV profiles and visualized using UMAP, and chromosomal CNV heatmaps were generated to illustrate CNV status across cells.

Spatial transcriptomic (ST) data collection and cell-type estimation

ST data for ESCC samples were obtained from GSE208253 [2]. Individual ST samples were pre-processed using the Seurat. To evaluate the spatial distribution of clusters identified in the scRNA-seq discovery cohort, ST and scRNA-seq expression matrices were integrated using CARD (v0.0.94), incorporating spatial coordinate.

Functional enrichment analysis of cell subclusters

Gene Ontology (GO) enrichment analysis for marker genes in each subcluster was performed using clusterProfiler (v4.6.0), with pathways considered significantly enriched at adjusted $P < 0.05$. Gene set variation analysis (GSVA) on hallmark pathways from MSigDB (v2023.2.Hs) was performed using the GSVA package (v1.34.0) to calculate GSVA scores.

Trajectory analysis

Fibroblast differentiation trajectories were inferred using Monocle3 (v1.3.4) with default parameters [3]. Trends were further validated using Monocle3. Epithelial cell trajectories were constructed using Monocle3 to outline evolutionary trends.

Gene set enrichment analysis and functional annotation

Gene Ontology (GO) and Kyoto Encyclopedia of Genes and Genomes (KEGG) enrichment analyses of differentially expressed genes (DEGs) were performed using the "ClusterProfiler" R package. The GO analysis encompassed three categories: cellular components, biological processes, and molecular functions. In addition, Gene Set Enrichment Analysis (GSEA) was conducted to explore pathways associated with different molecular subtypes, based on comprehensive gene sets from the Molecular Signatures Database (MSigDB).

Functional enrichment (GO and KEGG)

Differentially expressed and marker genes were subjected to GO and KEGG enrichment analyses using annotations from GO, UniProt, and NCBI. Significance was assessed by Fisher's exact test with FDR correction.

Cell-type identification by estimating relative subsets of RNA transcripts

To characterize the cellular composition of ESCC samples, we performed deconvolution analysis using CIBERSORTx (types from bulk transcriptomic data based on known gene–cell type associations [4]. For this analysis, the single-cell RNA-seq expression matrix was used to generate a signature matrix representing each cell population, while the TCGA-ESCC dataset served as the reference bulk transcriptomes. Estimated proportions of immune cell subsets were then used to characterize the immune landscape across patient groups. To assess potential associations with disease risk, Spearman correlation coefficients were calculated between the inferred immune cell fractions and corresponding risk scores. Comparative analyses and visualization of immune cell distributions and correlations were performed using the ggplot2 R package.

Statistical analysis

All of the statistical analyses were conducted via R software (version 4.2.0). Spearman's correlation was applied for the analysis of the correlation. The Wilcoxon test was used to compare the differences between these two risk groups. $p < 0.05$ was regarded as statistically significant.

Cell lines and cell culture

Human ESCC cell lines, including EC9706, KYSE150 and TE1, were sourced from the Shanghai Cell Bank of the Chinese Academy of Sciences (Shanghai, China). These cell lines were cultured in Dulbecco's Modified Eagle's Medium (DMEM) supplemented with 10% fetal bovine serum (FBS) (PAA Laboratories GmbH, Pasching, Austria) under standard conditions. All cells were maintained at 37 °C in a humidified incubator with 5% CO_2.

Western blot analysis

The anti-LAMA3 antibody used for Western blot analysis was purchased from Abcam (ab242197). Western blotting was carried out following established protocols. In brief, whole-cell lysates were extracted using RIPA buffer, and protein samples were resolved on 10% or 12.5% SDS-PAGE gels. The separated proteins were subsequently transferred onto PVDF membranes, which were then blocked with 5% non-fat milk in TBST (Tris-buffered saline with 0.1% Tween-20) for 1 h at room temperature prior to antibody incubation.

RNA interference

Short-interfering RNAs (siRNAs) targeting LAMA3 were purchased from Paiwei Biotechnology Co., Ltd. (Wuhan, China) and transfected into TE1 cells via Lipofectamine 2000 (Invitrogen, Shanghai, China) following the manufacturer's instructions. Scrambled siRNA served as a negative control. Forty-eight hours after transfection, the efficiency of gene knockdown was assessed via Western blot analysis.

Cell invasion and migration assays

Invasion and migration assays were performed using Transwell chambers (Corning, USA), with Matrigel coating applied for invasion assays and uncoated inserts used for migration assays. Cells were resuspended in medium containing 2% fetal bovine serum (FBS) and seeded into the upper chamber, while medium supplemented with 20% FBS was added to the lower chamber as a chemoattractant. After incubation at 37 °C for 24–48 h, non-migrated or non-invaded cells on the upper surface of the membrane were gently removed. Cells that traversed the membrane were fixed with methanol, stained with hematoxylin and eosin, and quantified in three randomly selected fields per insert under 100× magnification. Each experiment was independently repeated three times, and all functional assays were performed using three independent biological replicates ($n = 3$).

Introduction

Esophageal squamous cell carcinoma (ESCC) is a major histological subtype of esophageal cancer, accounting for more than 90% of cases in high-incidence regions such as East Asia [5, 6]. Despite improvements in treatment modalities, including surgery, chemotherapy, chemoradiotherapy, and immunotherapy, the prognosis for ESCC remains poor, with a 5-year survival rate of less than 25% [7–9]. In recent years, immunotherapy has emerged as a promising strategy in the treatment of esophageal cancer, particularly immune checkpoint inhibitors (ICIs) targeting PD-1 and PD-L1. However, a subset of patients exhibit resistance to immunotherapy, indicating that intratumoral heterogeneity and the tumor microenvironment (TME) play a crucial role in determining therapeutic efficacy [10–12]. Moreover, TME heterogeneity has been associated with different responses to treatment, including immunotherapy, which hampers the development of personalized therapeutic strategies.

Over the past decade, large-scale genomic and transcriptomic studies have revealed recurrent alterations in TP53, NOTCH1, and cell cycle-related genes in ESCC. However, these findings have not yet been translated into effective targeted therapies [13–15]. Recent studies have begun to unravel the complex landscape of the TME in ESCC, highlighting the roles of immune cells, cancer-associated fibroblasts (CAFs), and stromal components in tumor progression, immune evasion, and therapy resistance [16, 17]. Nevertheless, most of these insights have been derived from bulk RNA-seq or immunohistochemistry, which lack cellular resolution and spatial context [18]. The precise mechanisms by which specific

stromal or immune subsets influence ESCC progression, particularly in spatially distinct tumor regions, remain poorly understood.

The advent of single-cell RNA sequencing (scRNA-seq) and spatial transcriptomics (ST) has revolutionized our ability to dissect the cellular composition, functional states, and spatial organization of the TME at unprecedented resolution [19–21]. These technologies have provided valuable insights in multiple cancers, revealing distinct tumor subpopulations, immunosuppressive niches, and dynamic cell-cell interactions that shape tumor behavior. In ESCC, emerging single-cell studies have begun to delineate epithelial and immune cell diversity, but comprehensive integration with spatial data is still lacking. Such integrative approaches are essential to reveal context-dependent cell programs and to identify actionable vulnerabilities [22–25].

One area of particular interest is the invasive tumor front (ITF)-the dynamic interface between tumor and stroma-where active crosstalk occurs between malignant cells and the surrounding microenvironment. Recent evidence in other solid tumors has shown that the ITF harbors unique subpopulations of tumor and stromal cells that contribute to local invasion, metastasis, and immune modulation [26]. In ESCC, however, the cellular and spatial architecture of the ITF remains underexplored. A better understanding of spatial dynamics and molecular programs at the invasive front could provide critical insights into mechanisms of tumor dissemination and resistance, with direct implications for therapy.

This study integrates scRNA-seq and ST technologies to explore the TME of ESCC at multiple levels—transcriptional, epigenetic, and spatial—to unravel the complexity of the tumor microenvironment and its contribution to tumor progression and metastasis. By mapping the cellular landscape and identifying invasive-specific subpopulations, we aim to uncover novel biomarkers and therapeutic targets that may guide the development of more effective and personalized treatments for ESCC patients.

Result

Single-cell transcriptomics identified unique cellular composition patterns in esophageal cancer

To comprehensively elucidate the cellular characteristics of ESCC, we performed scRNA-seq analysis by integrating multiple cohorts of datasets [27, 28]. After filtering out putative doublets and low-quality or dying cells from the scRNA-seq data, A total of 208,446 cells from 24 esophageal cancer samples were clustered and categorized into 8 distinct clusters (Fig. 1A and B). Based on canonical marker genes, these clusters were annotated into eight major cell types: T and NK cells (*CD3D*, *CD3E*, *NKG7*; 69,497 cells, 33.3%), epithelial cells *(EPCAM*, *KRT19*; 43,301 cells, 20.8%), fibroblasts (*COL1A2*, *DCN*; 41,888 cells, 20.1%), myeloid cells (*MRC1*, *CD163*; 17,441 cells, 8.4%), B cells (*CD79A*, *MS4A1*; 13,692 cells, 6.6%), endothelial cells (*PECAM1*, *VWF*; 12,592 cells, 6.0%), plasma cells (*IGHA1*, *IGHG1*; 8,086 cells, 3.9%), and mast cells (*KIT*, *TPSB2*; 1,949 cells, 0.9%) (Fig. 1A and B). These 8 cell types were detected in almost every patient; however, their proportions varied greatly (Fig 1C). Spatial information is critical for understanding tumor biology; however, it is absent in scRNA-seq data. To address this, we performed spatial transcriptomics (ST-seq) on tissue sections from 12 ESCC patients to obtain in situ gene expression profiles. Tumor and non-tumor regions were delineated using the conditional autoregression-based deconvolution (CARD) algorithm (Fig. 1D and E). Furthermore, by integrating all single-cell populations into the spatial transcriptomic data through deconvolution, the distribution of distinct cell types could be clearly visualized across the tissue sections.

The LAMA3 + epithelial cell population underlies invasion and progression in ESCC

To identify the key cancer cell subclusters driving ESCC invasion, 42,999 epithelial cells were re-clustered into 10 subpopulations (Epithelial: C0–C9) (Fig. 2A and B). For each subcluster, the top five marker genes were identified, and functional annotation was performed based on highly expressed genes [29, 30]. C0 and C7 were enriched in ribosome biogenesis, translation, and energy metabolism, whereas C1 was characterized by lipid metabolism. C2 and C4 were associated with DNA replication and cell cycle progression, while C3 and C8 were linked to cell–matrix adhesion and extracellular matrix organization. C5 showed signatures of epithelial differentiation, C6 of iron homeostasis, and C9 of antigen processing and presentation (Fig. 2C). Further evaluation of gene enrichment revealed that the C3 subcluster exhibited high activity in epithelial–mesenchymal transition (EMT) and angiogenesis, suggesting a highly plastic epithelial state with strong differentiation potential toward invasive and pro-angiogenic phenotypes(Fig. 2C and D). To assess the malignant potential of epithelial subtypes, the "inferCNV" analysis was performed using endothelial cells as the reference [17, 19]. Compared with normal epithelial cells, most clusters displayed evident CNV alterations. Subclusters C7, C8, and C9 showed relatively low CNV scores, indicative of largely normal epithelial populations, whereas C3 exhibited intermediate CNV scores, consistent with a moderately malignant phenotype (Fig. 2E). Considering its strong EMT signature, C3 likely represents a trans-differentiating epithelial state with modest malignancy but pronounced EMT potential [31, 32]. The C3 subcluster was further marked by high expression of *LAMA3*, *COL17A1*, *LAMC2*, *INHBA*, and

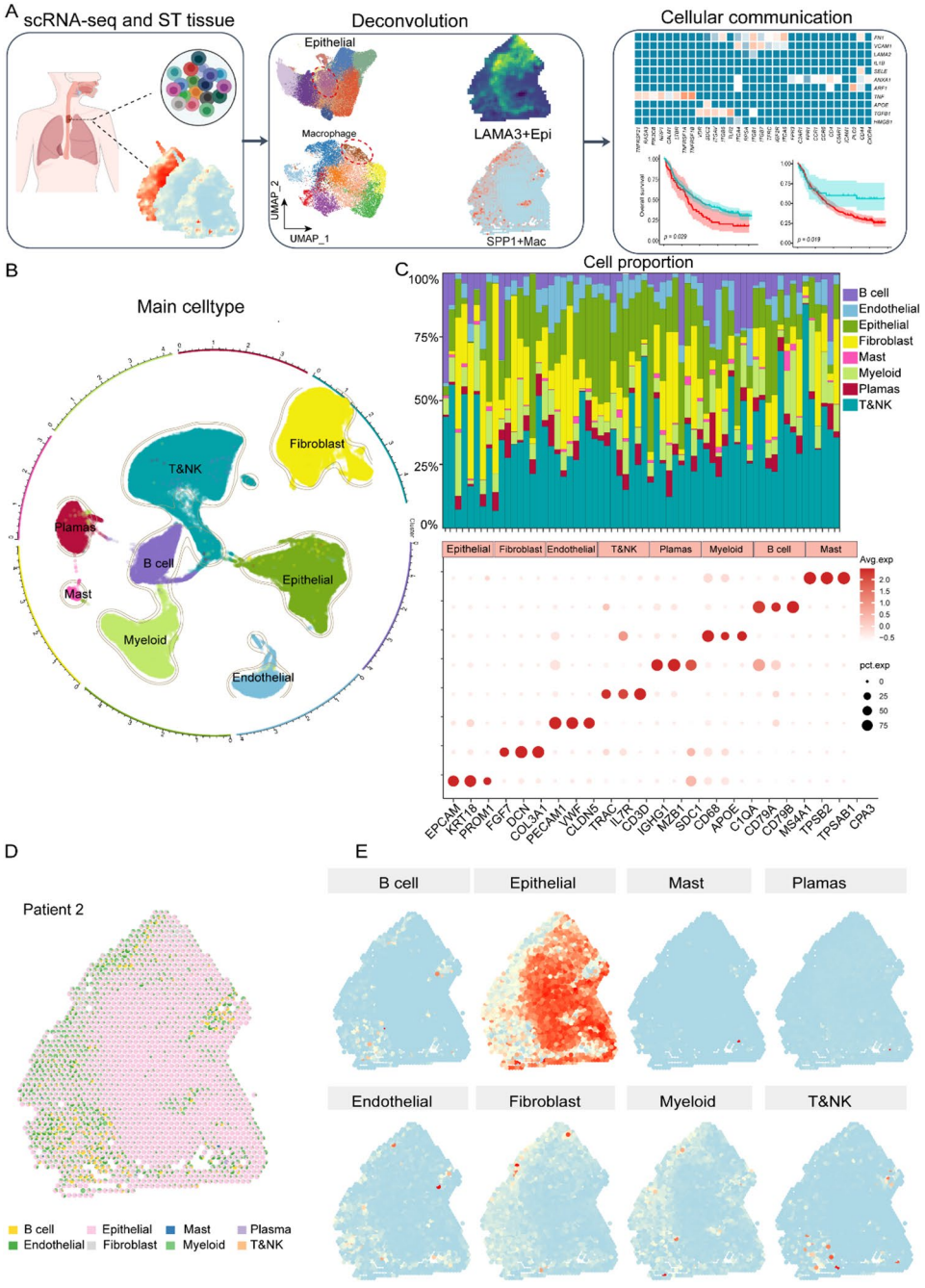

Fig. 1 Integrative characterization of the cellular landscape of the ESCC microenvironment using single-cell and spatial transcriptomics. (**A**) Schematic illustration of tissue dissociation, cell isolation, sequencing, and downstream bioinformatics analysis. (**B**) UMAP visualization of ESCC, with the inner ring representing major cell types and the outer ring indicating tissue-of-origin proportions. (**C**) Stacked bar plot showing the cellular composition of each ESCC sample. (**C**) Dot plot displaying canonical marker gene expression across the major cell types. (**D**) Spatial distribution of eight cell types on ST sections from ESCC tissues (n = 12), with pie charts representing the cellular composition of each spot. (**E**) Spatial distribution of representative cell types in the ST dataset, where yellow shading indicates higher expression of the corresponding genes within each spot

TNC. When mapped onto spatial tissue sections, these LAMA3 + epithelial cells were predominantly localized at the tumor margins, indicating spatially specific distribution (Fig. 2F). Using spatial transcriptomics data, we observed a significant positive correlation between LAMA3 + epithelial cells and EMT activity ($R = 0.65$, $p < 0.01$), corroborating their strong EMT potential (Fig. 2G). Analysis of TCGA-ESCC data further demonstrated that high expression of LAMA3 + epithelial cell signatures was significantly associated with poor patient prognosis (Fig. 2H). Together, these findings highlight C3 as a trans-differentiating, invasion-prone epithelial subpopulation

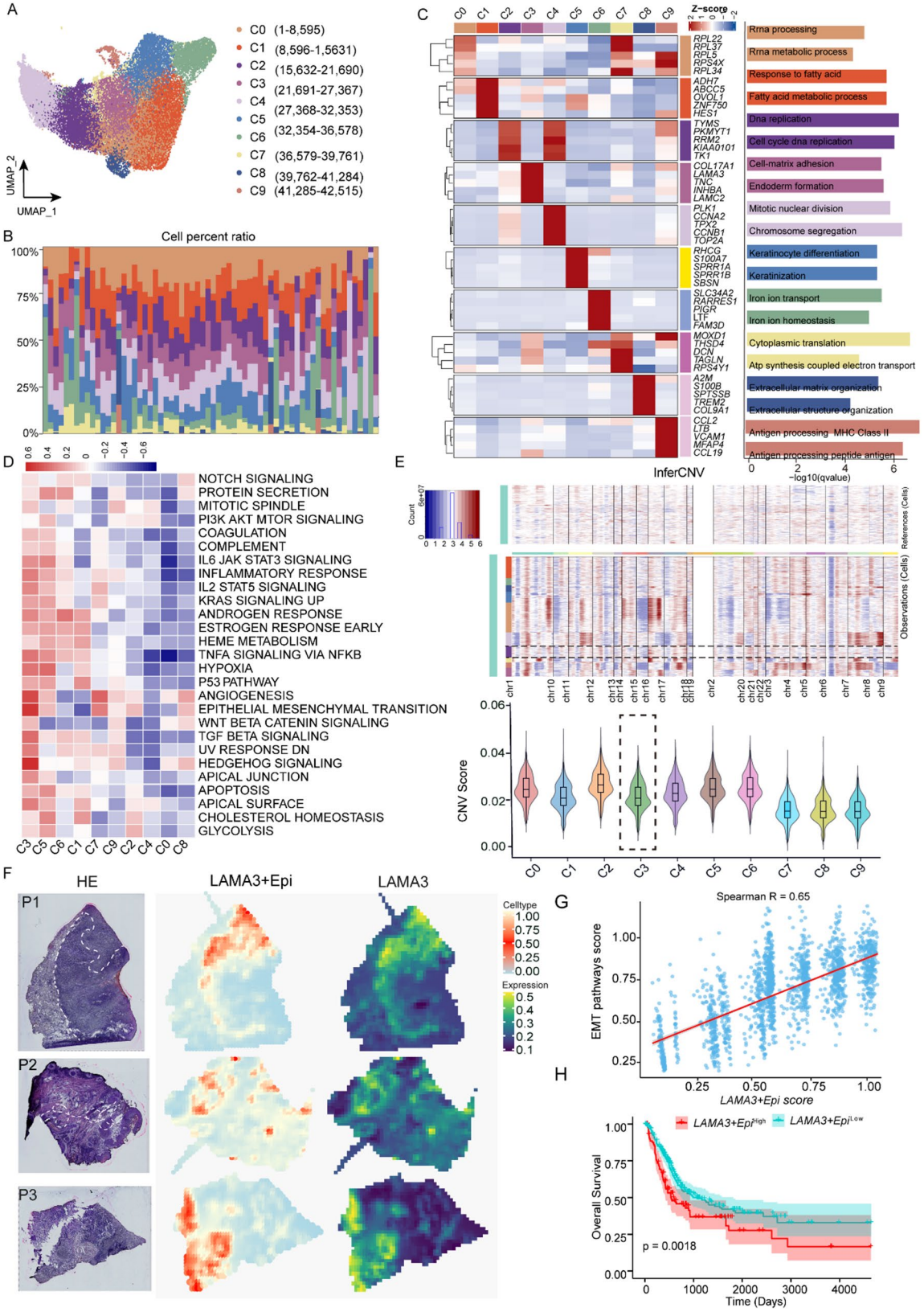

Fig. 2 (See legend on next page.)

(See figure on previous page.)

Fig. 2 Characterization of epithelial cell heterogeneity, functional states, and clinical relevance in ESCC. (**A**) UMAP of epithelial cells and cell type annotation. (**B**) Stacked bar plot showing the epithelial cells subpopulation composition of each ESCC sample. (**C**) Heatmap displaying the top five discriminative genes for 10 different cell types. The box on the right presents the GO enrichment analysis results for the marker genes. (**D**) Gene set variation analysis (GSVA) of Hallmark pathways across epithelial cell subpopulations. (**E**) Heatmap showing large-scale CNVs in epithelial cells the normalized CNV levels are shown; red represents a high CNV level, and blue represents a low CNV level (top). The CNV score of the subpopulation of epithelial cells. (**F**) Spatial distribution of representative cell types in the ST dataset, where yellow shading indicates higher expression of the corresponding genes within each spot. (**G**) Scatter plots show the correlation between the LAMA3+ epithelial cells and EMT score in the patients. (**H**) Kaplan–Meier survival curves showing overall survival in the TCGA-ESCC cohort, stratified by high versus low infiltration of the LAMA3+ epithelial cells. Statistical significance was assessed using the log-rank test

with spatial specificity at tumor margins and clinical relevance in ESCC progression.

Identification of seven fibroblast subtypes and their evolutionary trajectories and transcriptional regulatory features in ESCC

To elucidate the pivotal role of fibroblasts in shaping the ESCC microenvironment, we utilized previously reported fibroblast subtype-specific markers and categorized 21,629 fibroblasts into seven clusters: H2AFZ+ fibroblasts, MMP3 + fibroblasts, PTGDS+ fibroblasts, PLA2G2A+fibroblasts, RGS5 + fibroblasts, CLEC3B+fibroblasts, SFRP4 + fibroblasts (Fig. 3A and B). The distribution of fibroblast subtypes was further projected onto the spatial transcriptomics data, enabling visualization of their localization within the ESCC tumor microenvironment. We observed that RGS5 + Fib, MMP3 + Fib, SFRP4 + Fib, and CLEC3B + Fib were sparsely distributed across spatial sections, while PLA2G2A + Fib were predominantly enriched in stromal regions. In contrast, H2AFZ + Fib were mainly localized within tumor regions, and PTGDS + Fib were also broadly expressed in tumor areas Fig. 3C. To comprehensively evaluate their clinical significance, we next investigated the prognostic relevance of all fibroblast subtypes using TCGA-ESCC bulk RNA-seq data with the "CIBERSORTx" algorithm. Among these subtypes, high infiltration of H2AFZ+ fibroblasts was significantly associated with poorer overall survival in ESCC patients ($p = 0.049$), and elevated infiltration of PTGDS+ fibroblasts was similarly correlated with unfavorable prognosis ($p = 0.0028$), whereas the remaining subtypes showed no significant prognostic impact (Fig. 3D). To investigate the dynamic processes of fibroblast subtypes at single-cell resolution, we performed pseudo-time trajectory analysis. The analysis revealed major trajectories, with CLEC3B+ fibroblasts exhibiting the highest Potency score, suggesting that this subtype possesses the greatest differentiation potential and ultimately evolves into RGS5 + fibroblasts (Fig. 3E). Along the pseudo-time trajectory, the expression of *WISP2* gradually decreased, whereas *FGF7* and *VCAN* were expressed in both the initial and inflammatory states. Additionally, ECM-related genes, such as *ACTG2*, showed elevated expression at the terminal stage. Gene expression dynamics during state transitions were visualized in a smoothed heatmap (Fig. 3F). Functionally, genes expressed in the early stage were enriched in pathways associated with extracellular matrix organization, vascular development, and complement activation, reflecting a tissue-structuring and immune-modulatory role. As pseudo-time progressed, gene expression shifted toward pathways related to collagen organization, ECM remodeling, and mononuclear cell migration, indicating active extracellular matrix remodeling and interactions with immune cells. At the terminal stage, the gene programs highlighted cell cycle and mitotic processes, suggesting that fibroblasts at this stage may contribute to tumor progression (Fig. 3G).

Tumor-specific SPP1 + macrophages are associated with ESCC progression

The remodeling of myeloid cells in ESCC patients indicates that these cells may exert functional roles in tumorigenesis. A total of 14,887 myeloid cells were analyzed and classified into ten distinct subpopulations. Two dendritic cell (DC) subsets were identified, namely HLA-DQB2 + DCs and CST7 + DCs, six macrophage subtypes were characterized, including RGS1 + Mac, TYMS + Mac, SPP1 + Mac, IFITM + Mac, SEPP1 + Mac, and TGFBI + Mac, while two neutrophil populations were defined as S100A8 + Neu and MT2A + Neu (Fig. 4A). Notably, the relative abundance of these myeloid subsets varied substantially across patients, reflecting considerable inter-patient heterogeneity (Fig. 4B and C). Given that macrophage polarization can be broadly categorized into classically activated M1 and alternatively activated M2 phenotypes, we next evaluated the polarization status of the six macrophage subsets using M1/M2 signature scoring. The results revealed that, except for SEPP1 + Mac and SPP1 + Mac, which exhibited an M2-like phenotype, the remaining macrophage subsets predominantly displayed M1-like characteristics (Fig. 4D). The distribution of macrophage subtypes was further projected onto the spatial transcriptomics data, enabling visualization of their localization within the ESCC tumor microenvironment. We observed that SPP1 + macrophages displayed a distinct spatial distribution pattern, with high expression restricted to stromal regions at the tumor boundary (Figure. 4E).

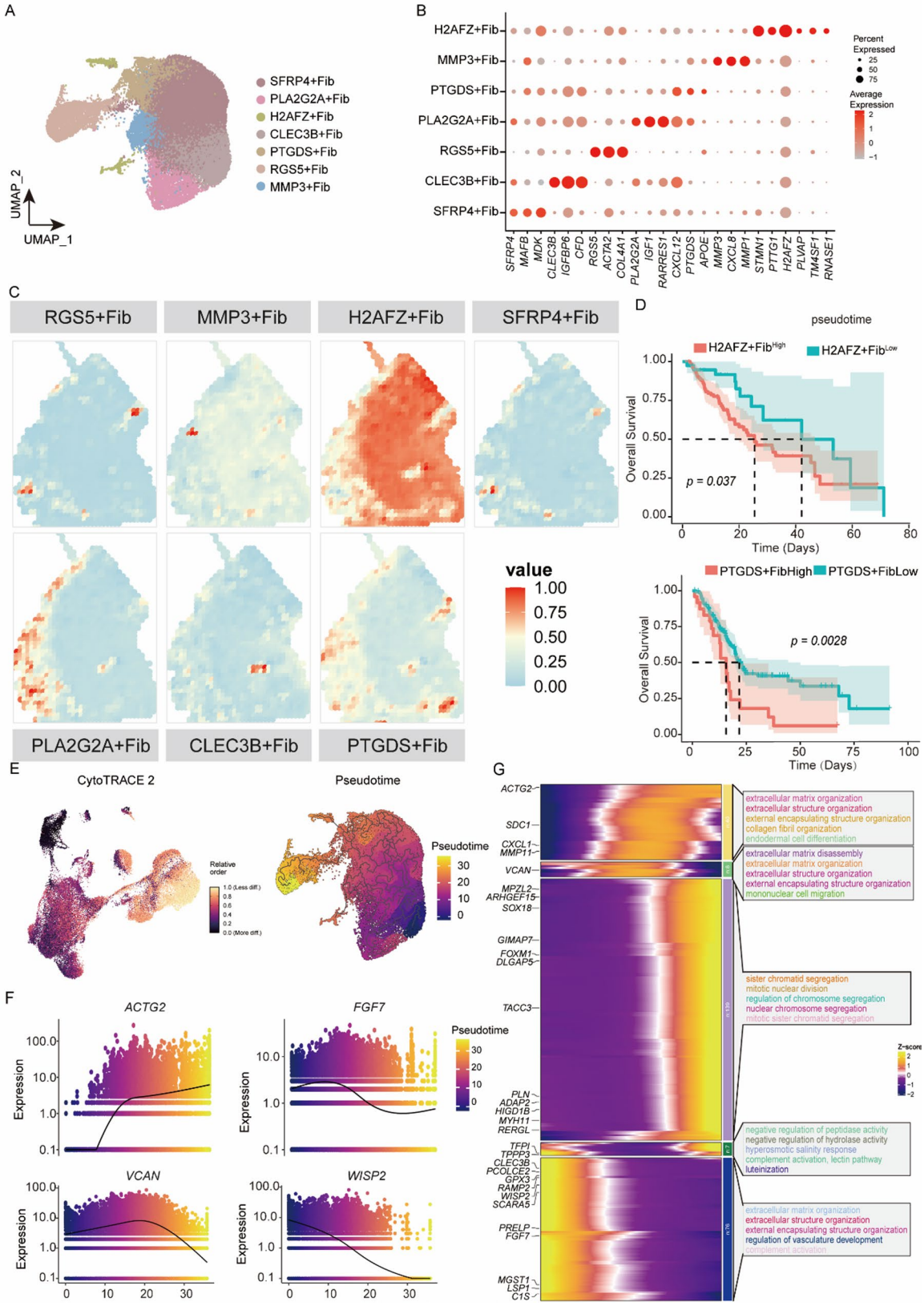

Fig. 3 (See legend on next page.)

(See figure on previous page.)

Fig. 3 Dynamic transcriptional programs and prognostic value of fibroblasts in ESCC. (**A**) UMAP plot shows the distribution of fibroblast cells across ESCC samples. (**B**) Dot plot presents the top three marker genes for each fibroblast subtype. (**C**) Spatial distribution of fibroblasts subpopulation in the ST dataset, where yellow shading indicates higher expression of the corresponding genes within each spot. (**D**) Kaplan–Meier survival curves of TCGA ESCC cohorts, stratified by high versus low infiltration of H2AFZ+ fibroblast and PTGDS+ fibroblast clusters. Statistical significance was determined using the log-rank test. (**E**) Inferred cell trajectory tree and pseudo-time ordering of fibroblasts. Cells with high stemness scores predicted by "CytoTRACE" are shown (left), and the proportions of fibroblasts in different states along pseudo-time inferred by Monocle3 are displayed (right). (**F**) Expression dynamics of representative genes along the pseudo-time trajectory. (**G**) Heatmaps illustrate gene expression patterns and cellular modules of fibroblasts associated with pseudo-time progression.

We next compared spots with high versus low SPP1 expression, and pathway enrichment analysis revealed activation of multiple oncogenic and immune-regulatory signaling cascades. These included pathways related to ribosome biogenesis and cell cycle progression, as well as cancer-associated signaling networks such as MAPK, P53, *TGF-β*, Hippo, JAK-STAT, and NF-κB. Collectively, these results suggest that SPP1-enriched regions are characterized by enhanced proliferative activity, malignant signaling, and immunomodulatory processes within the ESCC tumor microenvironment (Fig. 4 F). To further elucidate the functional role of SPP1 + macrophages in ESCC, we performed deconvolution analysis of bulk RNA-seq data from the TCGA-ESCC cohort. The analysis demonstrated a significantly higher proportion of SPP1 + macrophages in tumor tissues compared to adjacent non-tumor tissues (Fig. 4G). Importantly, increased infiltration of SPP1 + macrophages was strongly associated with unfavorable prognosis (Fig. 4H). Moreover, deconvolution of multiple immunotherapy cohorts revealed that enrichment of SPP1 + macrophages was indicative of an immunosuppressive tumor microenvironment, suggesting their potential contribution to immune evasion in ESCC (Fig. 4I).

Co-occurrence of LAMA3 + epithelial cells and SPP1 + macrophages predict impaired response to anti–PD-L1 immunotherapy

To investigate the infiltration status of these cellular subsets, we applied a spatial transcriptomics–based deconvolution approach to estimate the abundance of 27 cell clusters identified by scRNA-seq and further calculated the pairwise Spearman correlations of their infiltration levels in each patient. We found that LAMA3 + epithelial cells and SPP1 + macrophages consistently represented the most strongly correlated populations across all examined patients (Fig. 5A). Given the limited sample size of our ST dataset, we next employed "CIBERSORTx" to simulate cell-type-specific gene expression profiles and predict the relative abundance of scRNA-seq–defined cell types in larger datasets, including the TCGA ESCC cohort and five independent ESCC cohorts from GEO. The deconvolution robustness of "CIBERSORTx" was validated by training with our own scRNA-seq dataset. Strikingly, across all interrogated cohorts, we consistently observed a significant positive correlation between LAMA3 + epithelial cells and SPP1 + macrophages, further confirming their close association (Fig. 5B). Since current tumor immunotherapies predominantly target lymphocytes, reduced lymphocyte infiltration in these tumors may weaken therapeutic efficacy. To test this hypothesis, we analyzed the IMvigor210 cohort of bladder cancer patients treated with anti–PD-L1 therapy. Patients with higher proportions of LAMA3 + epithelial cells or SPP1 + macrophages, as estimated by cell-type deconvolution, exhibited significantly worse overall survival (OS) compared with those with lower proportions. Moreover, patients with concomitantly high proportions of LAMA3 + epithelial cells and SPP1 + macrophages showed the shortest survival times. Importantly, individuals with elevated proportions of either LAMA3 + epithelial cells or SPP1 + macrophages displayed markedly lower response rates (CR/PR) and higher frequencies of progressive disease (PD) than those with low proportions of both cell types (Fig. 5C and 5D). Together, these findings reveal a conserved co-occurrence of LAMA3 + epithelial cells and SPP1 + macrophages across multiple cancer types and suggest that enrichment of these cell subsets may contribute to reduced lymphocyte infiltration and impaired responses to anti–PD-L1 immunotherapy.

LAMA3 + epithelial cells and SPP1 + macrophages interaction may contribute to desmoplastic tumor microenvironment

We next investigated whether LAMA3 + epithelial cells and SPP1 + macrophages spatially colocalize in ESCC tissues. Immunofluorescent staining confirmed the close proximity of these two populations, suggesting potential crosstalk between them (Fig. 6A). To further explore the underlying mechanisms, we applied the R package "NicheNet" to infer ligand–receptor interactions [33]. This analysis revealed that LAMA3 + epithelial cells could directly interact with SPP1 + macrophages through adhesive ligand–receptor pairs, such as *VCAM1–ITGB1*, *TNF–TNFRSF1A/TNFRSF1B*, and *ARF1–PLD2* (Fig. 6B). Moreover, LAMA3 + epithelial cells were predicted to enhance the pro-inflammatory activity of SPP1 + macrophages by expressing TGF-β superfamily members, which in turn induced signaling via *ACVRL1*, *ACVR1*, and *ACVR1B* in SPP1 + macrophages. To assess whether SPP1 + macrophages regulate ECM-remodeling functions, we again performed NicheNet analysis. SPP1 +

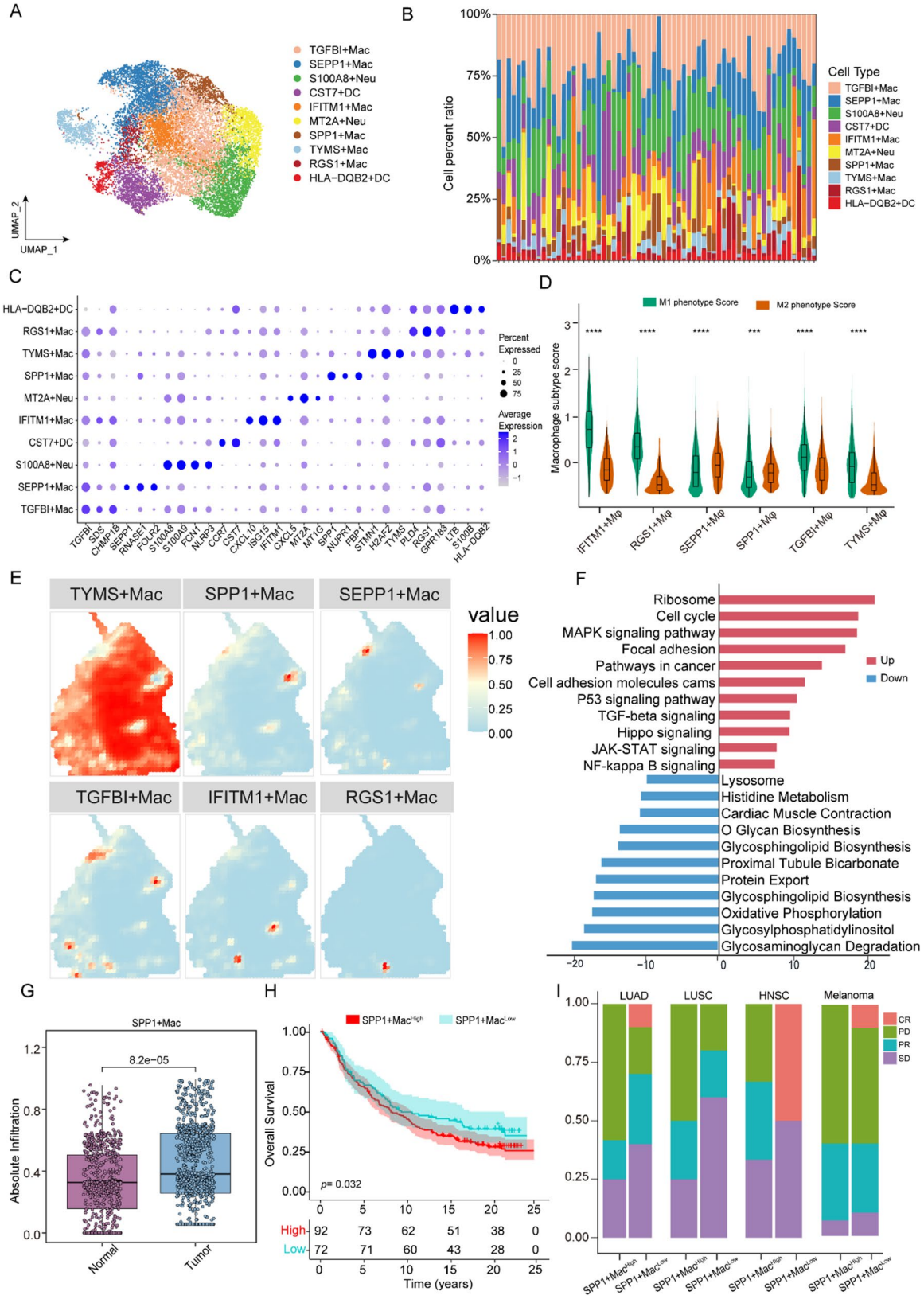

Fig. 4 (See legend on next page.)

(See figure on previous page.)

Fig. 4 Single-cell characterization of myeloid cell diversity associated with ESCC. (**A**) UMAP plot shows the distribution of myeloid cells from ESCC patients. (**B**) Stacked bar plot depicting cell type composition in each sample from ESCC. (**C**) Dotplot of the marker genes identified for each myeloid cell type. (**D**) Comparison of average M1 and M2 scores among macrophages, indicating a shift toward M2-like polarization. (**E**) Spatial distribution subpopulation of macrophages in the ST dataset, where yellow shading indicates higher expression of the corresponding genes within each spot. (**F**) Differential gene expression analysis between spots enriched with SPP1+ macrophages and those without such enrichment. (**G**) Comparison of SPP1+ macrophage percentages in paired normal and tumor tissue. (**H**) Kaplan–Meier survival curves showing overall survival in the ESCC cohort, stratified by high versus low infiltration of the specified SPP1+macrophage cell clusters. Statistical significance was assessed using the log-rank test. (**I**) Deconvolution analysis of SPP1+ macrophages in relation to tumor immunotherapy responses

macrophages showed strong ligand activity for *TGFB1*, *IL1B*, and *IL6*, which were predicted to interact with corresponding receptors on LAMA3 + epithelial cells. These interactions induced the expression of pro-fibrotic and ECM-related genes in epithelial cells, including VCAM1, *ITGA4*, *ADAM17*, and *TGFB-1*, many of which are central mediators of ECM production and remodeling. Thus, SPP1 + macrophages may drive ECM deposition and desmoplastic formation by activating LAMA3 + epithelial cells through TGFB1- and IL1B/IL6-dependent signaling pathways. To further characterize the downstream biological effects, we conducted "NicheNet" ligand activity analysis using KEGG ECM-related gene sets. The predicted target genes were enriched in multiple pathways, including cytokine-mediated signaling, leukocyte cell–cell adhesion, regulation of apoptotic signaling, response to oxidative stress, and response to interferon-γ. These pathways provide mechanistic links between ligands secreted by SPP1 + macrophages and ECM-target genes that contribute to desmoplastic remodeling (Fig. 6C and D). Taken together, these findings demonstrate that LAMA3 + epithelial cells and SPP1 + macrophages form a reciprocal interaction network that reinforces their maintenance and function. By cooperating with LAMA3 + epithelial cells, these cell populations may play pivotal roles in ECM remodeling and the development of desmoplastic regions within the ESCC tumor microenvironment, thereby shaping tumor progression and potentially influencing therapeutic responses.

Dual role of LAMA3 in shaping the immune microenvironment and driving tumor progression

The tumor immune microenvironment (TIME) is generally categorized into three types based on immune cell and CD8 + T-cell infiltration: immune-excluded, inflamed (or "hot" tumors, which typically respond well to immunotherapy), and immune-desert. To better understand the immune context of tumors with distinct infiltration patterns of LAMA3 + epithelial cells and/or SPP1 + macrophages, we examined the immune features of ESCC subtypes. Notably, ESCC tumors with high LAMA3 + epithelial cell and high SPP1 + macrophage infiltration exhibited a relatively elevated burden of non-silent mutations and SNV-predicted neoantigens. They also displayed a higher Shannon entropy index and greater TCR richness, reflecting a non-effective T-cell response to neoantigens (Fig. 7A). Paradoxically, this subtype had the lowest lymphocyte infiltration among all ESCC groups, suggesting an immunologically "cold" tumor phenotype despite harboring immunogenic mutations. To further explore the oncogenic role of LAMA3, we assessed its expression in multiple ESCC cell lines (EC9706, KYSE150 and TE1). LAMA3 mRNA was markedly upregulated in tumor cell lines, especially in TE1 cells (Fig. 7B), which were therefore selected for downstream experiments. Functional assays confirmed efficient knockdown of LAMA3 in TE1 cells (Fig. 7C). The colony formation assay demonstrated that silencing LAMA3 significantly reduced the number and size of cell colonies compared with the control group, indicating that LAMA3 promotes the long-term proliferative capacity and clonogenicity of ESCC cells. ($p < 0.01$) (Fig. 7D). Phenotypic assays demonstrated that LAMA3 knockdown markedly suppressed oncogenic behaviors: Transwell assays showed impaired migration and invasion, while wound-healing assays confirmed reduced migratory ability (Fig. 7E, F). Consistently, EdU assay indicated that knockdown of LAMA3 significantly inhibited the viability of ESCC cells(Fig. 7G). Collectively, these findings highlight LAMA3 as a potential oncogenic driver and therapeutic target in ESCC, functioning to enhance proliferation, migration, and invasion.

Discussion

The tumor microenvironment (TME) of ESCC is highly heterogeneous and plays a central role in tumor progression, immune evasion, and therapeutic resistance. Our integrative analysis of single-cell and spatial transcriptomics delineated the complex cellular ecosystem of ESCC and uncovered novel malignant and stromal subpopulations with spatial and functional specificity. These findings underscore the importance of dissecting TME heterogeneity to better understand ESCC biology and to identify new therapeutic opportunities.

A key finding of our study is the identification of a LAMA3 + epithelial subpopulation enriched at the invasive tumor front (ITF). This population exhibited strong epithelial–mesenchymal transition (EMT) signatures, angiogenesis potential, and intermediate CNV alterations, suggesting a trans-differentiating state with modest malignancy but pronounced invasive capacity. The spatial restriction of LAMA3 + cells to tumor margins highlights their functional role in driving local invasion.

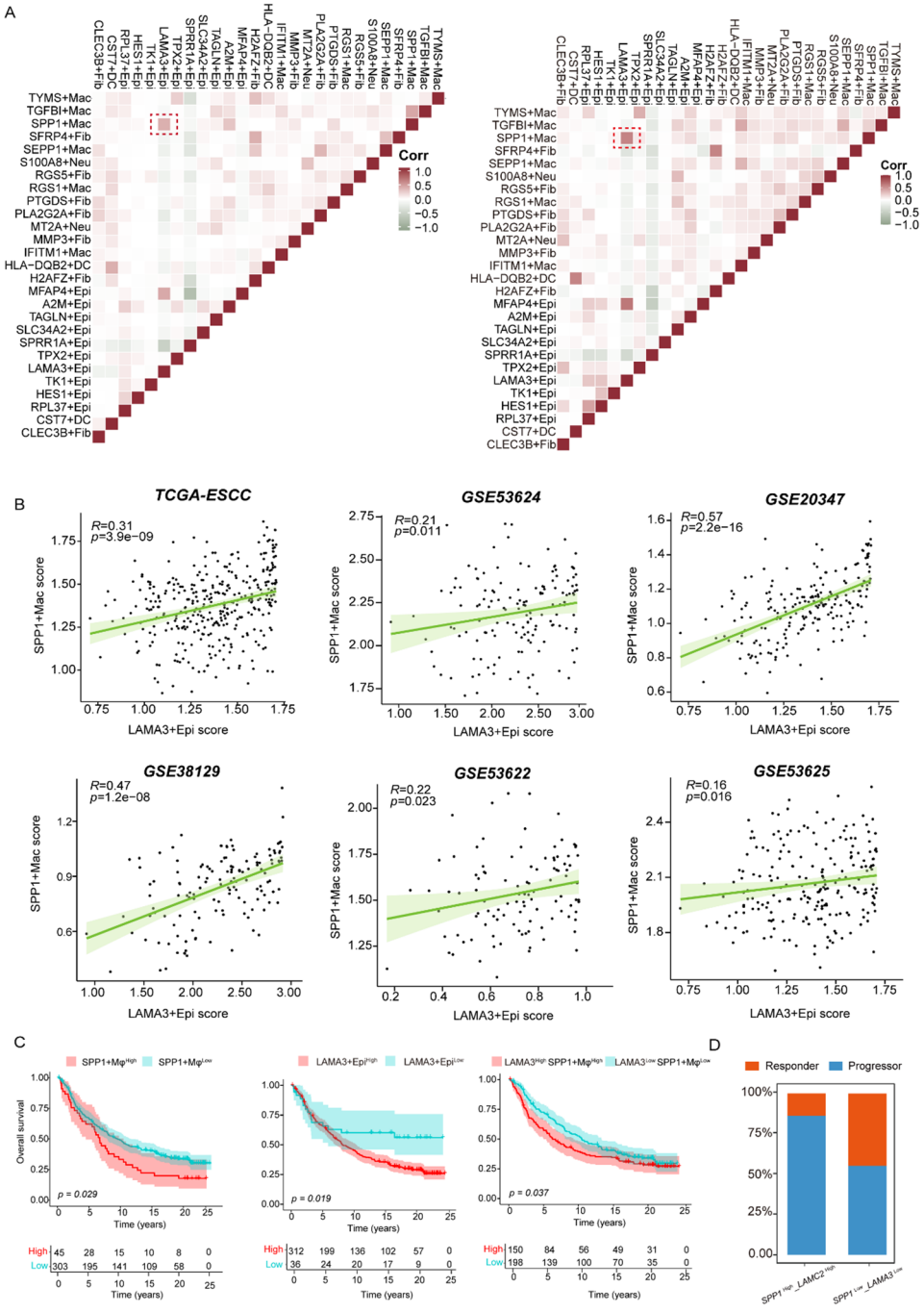

Fig. 5 Correlation of stromal and myeloid cell infiltration and prognostic relevance of LAMA3/SPP1 in ESCC and immunotherapy cohorts. (**A**) The proportion of ESCC cohorts with positive (Spearman correlation; correlation coefficient [Rs] >0.3 and FDR < 0.05, in red), negative (Rs < −0.3 and FDR < 0.05, in blue), or non-significant (gray) correlation for the infiltration of pairwise cell types. (**B**) Scatter plots show the correlation between the infiltration of LAMA3 + epithelial cells and SPP1 + macrophages across 6 independent datasets with ESCC, including TCGA-ESCC; GSE53624; GSE20347; GSE38129; GSE53622; GSE53625. The error band indicates 95% confidence interval. (**C**) Survival analyses for low and high expression of LAMA3 alone, SPP1 alone, and both. patient groups in the anti-PD-L1 immunotherapy cohort using Kaplan–Meier curves (IMvigor210 cohort). (D) Bar plots show patients with both low expression of LAMA3 and SPP1 are more likely to respond to anti-PD-L1 treatment

Moreover, their expression signature was consistently associated with poor prognosis in ESCC and other cancers, implicating LAMA3 as a conserved marker of aggressive tumor states [34, 35]. Functionally, our in vitro experiments further demonstrated that LAMA3 knockdown impaired proliferation, migration, and invasion, establishing LAMA3 as not only a marker but also a potential oncogenic driver.

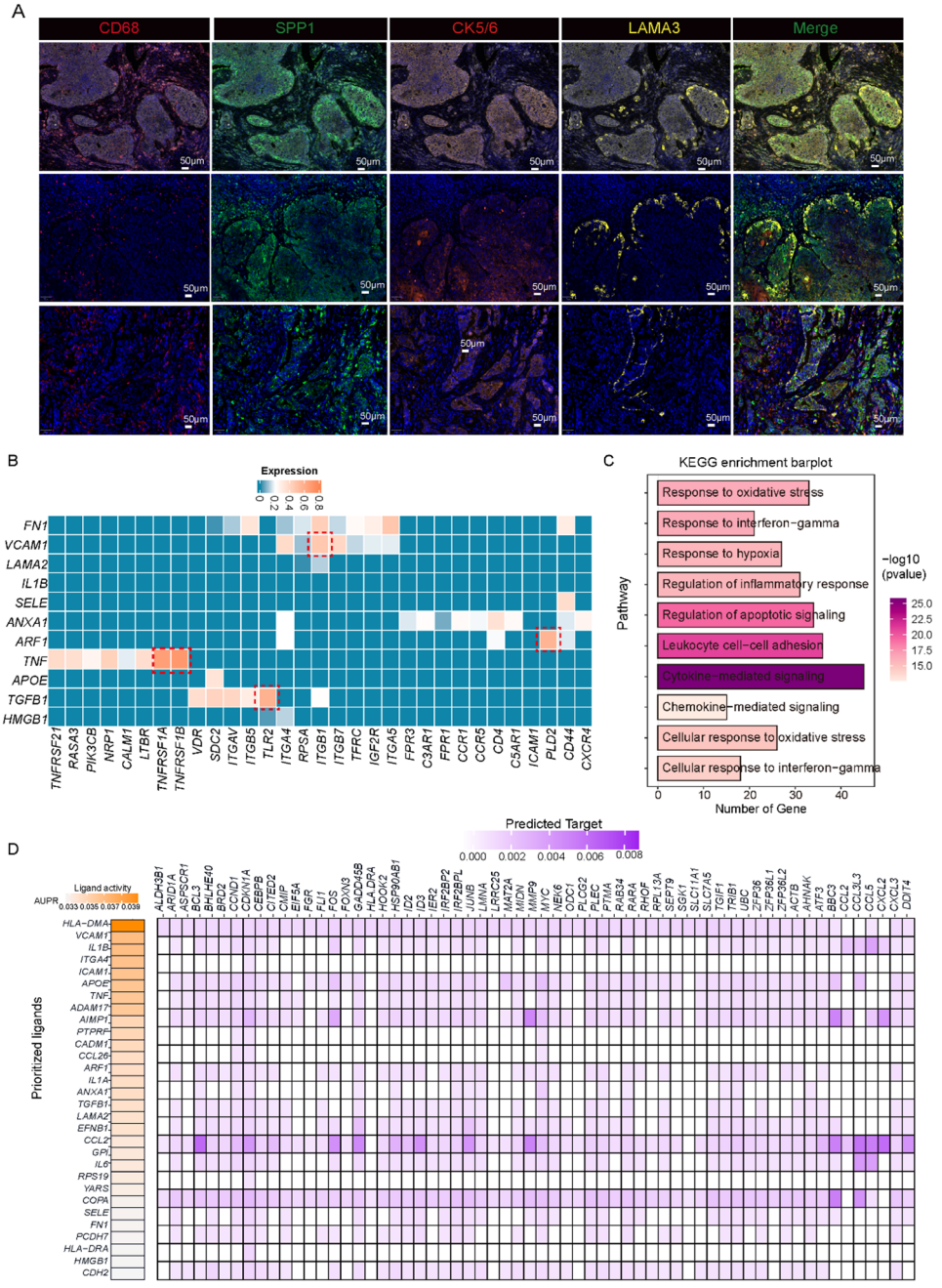

Fig. 6 The LAMA3 + epithelial cell and SPP1 + macrophages interaction may contribute to desmoplastic tumor microenvironment. (**A**) Representative IF staining of ESCC tissue (20x). DAPI (blue), CD68 (pink), SPP1 (green),CK5/6c (red), LAMA3 (yellow) in individual and merged channels are shown. Bar, 50 μm. Experiment was performed in three independent patients. (**B**) a Heatmap of top predicated ligands expression across subtypes of NicheNet which was used to predicate ligands expressed by LAMA3+ epithelial cell that modulate SPP1+ macrophages. (**C**) Representative KEGG pathways enrichment of the predicted target genes expressed in LAMA3+ epithelial cell. The statistical analysis was performed by Fisher's test. (**D**) in each myeloid subtype. Ligand-receptor pairs showing interaction between SPP1+ macrophages and LAMA3+ epithelial cell ordered by ligand activity. The Heatmap showing regulatory potential of top 20 ranked ligand and the downstream target genes in LAMA3+ epithelial cell

In addition to malignant epithelial cells, we identified seven fibroblast subtypes with distinct developmental trajectories and transcriptional programs. The dynamic transitions revealed by pseudo-time analysis reflected a progression from vascular-associated fibroblasts to ECM-remodeling fibroblasts. Notably, terminal fibroblast states were enriched in ECM-remodeling and TGF-β signaling, processes known to foster desmoplasia and therapeutic resistance. Prognostic analysis indicated that infiltration of H2AFZ+ fibroblasts was linked to worse

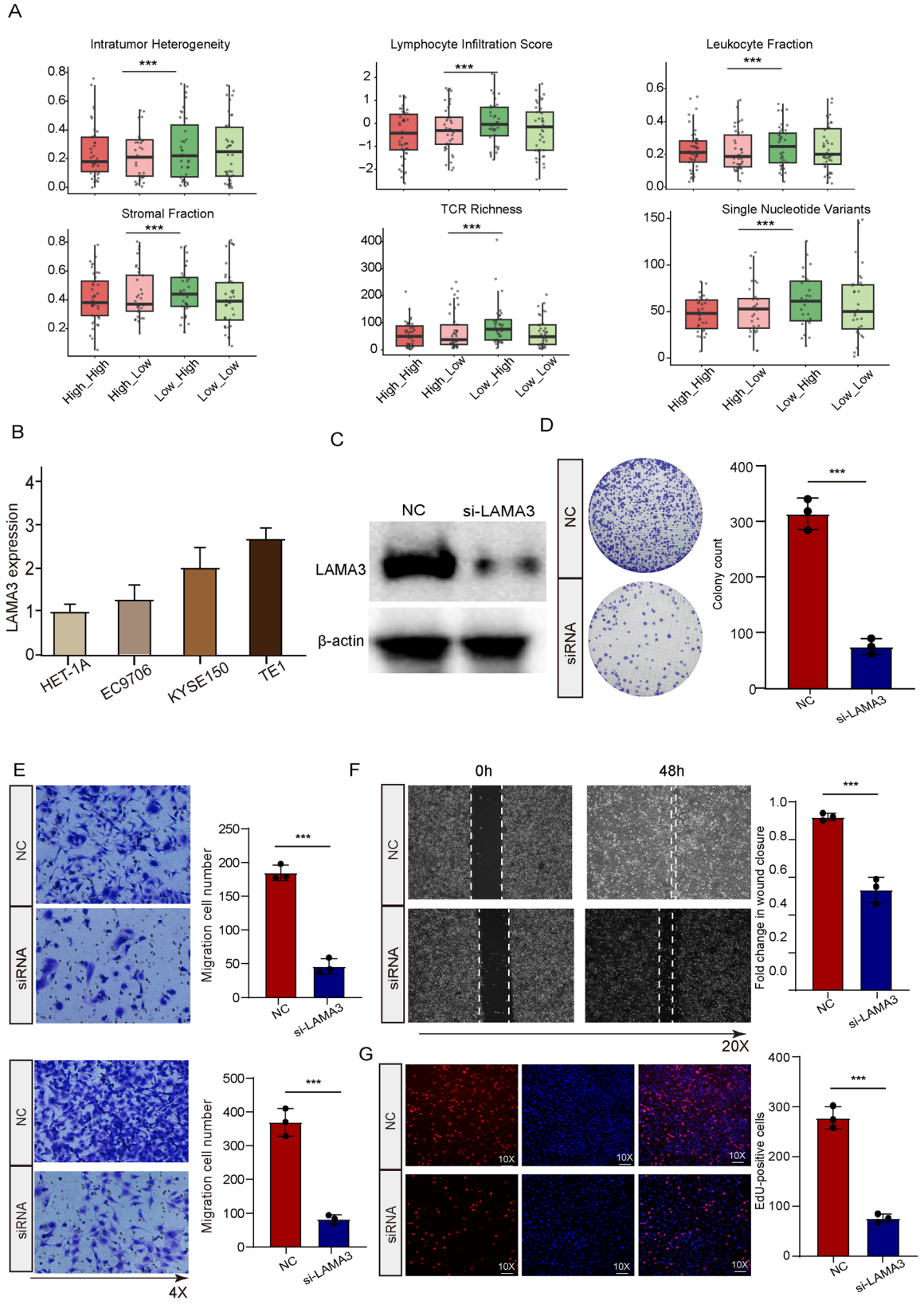

Fig. 7 Additional labels (D, F, and G) have been included to provide a clearer presentation of the results

survival, supporting their clinical relevance. These results emphasize the plasticity of fibroblasts in ESCC and their contribution to stromal remodeling, which may cooperate with malignant epithelial states to drive invasion.

Our study also uncovered a tumor-enriched SPP1⁺ macrophage population that, while showing a predominantly M2-like phenotype in our dataset, has been reported to exhibit M1 phenotypes in other studies, and was strongly associated with poor prognosis and reduced immunotherapy response. Deconvolution across multiple cohorts confirmed their enrichment in ESCC tumors compared with adjacent tissues, highlighting their robustness as a TME feature. Importantly, we observed a strong spatial and transcriptional association between SPP1 + macrophages and LAMA3 + epithelial cells. This co-occurrence predicted impaired responses to anti–PD-L1 therapy, not only in ESCC but also in independent immunotherapy cohorts, suggesting a conserved mechanism of resistance [36–39].

Mechanistically, our "NicheNet" analysis suggested that LAMA3 + epithelial cells and SPP1 + macrophages engage in reciprocal crosstalk through adhesive ligand–receptor interactions and cytokine signaling, promoting fibroblast activation, ECM deposition, and desmoplastic remodeling. This cooperative network may generate a rigid, immune-excluded microenvironment that restricts lymphocyte infiltration, thereby explaining the paradoxical observation of high mutational burden but poor immune response in ESCC tumors with LAMA3 + and SPP1 + enrichment. Thus, our data propose a model in which LAMA3 + epithelial cells and SPP1 + macrophages synergistically establish an immunosuppressive and desmoplastic niche that facilitates invasion and therapy resistance [36, 38, 40].

Several limitations should be acknowledged. The spatial transcriptomics analyses were based on cross-sectional data from a relatively small ESCC cohort and partially relied on public datasets, which may introduce bias and limit generalizability. Despite rigorous normalization and batch-correction procedures, residual batch effects cannot be fully excluded. Functional evidence for SPP1⁺ macrophages and the LAMA3–SPP1 axis is currently limited to in vitro assays, and in vivo validation remains necessary. In addition, the resolution of spatial transcriptomic spots may not fully capture cell–cell interactions at single-cell precision. While SPP1⁺ macrophages have been reported previously, our study extends existing knowledge by providing mechanistic insight into the role of the LAMA3–SPP1 axis in desmoplasia and immune evasion in ESCC. Taken together, our study highlights the invasive tumor front as a critical niche in ESCC, characterized by the convergence of invasion-prone epithelial cells, immunosuppressive macrophages, and activated fibroblasts. The co-occurrence of LAMA3 + epithelial cells and SPP1 + macrophages emerge as a robust biomarker of poor prognosis and immunotherapy resistance. Therapeutically, strategies targeting this axis—such as disrupting epithelial–macrophage interactions, inhibiting LAMA3 signaling, or reprogramming SPP1 + macrophages—may represent promising avenues to overcome desmoplasia and improve immunotherapy efficacy in ESCC.

Supplementary Information

The online version contains supplementary material available at https://doi.org/10.1186/s12967-026-08004-5.

Supplementary Material 1

Supplementary Material 2

Supplementary Material 3

Acknowledgements
None.

Author contributions
K.H. and C.P. contributed equally to this work. K.H. performed the majority of experiments, conducted bioinformatic analyses, and wrote the manuscript. C.P. contributed to experiments and data analysis. Y.Z. and Y.D. assisted in experimental design and data interpretation. J.Q. and P.W. supervised the study, conceived and guided the project, and revised the manuscript. All authors discussed the results and approved the final manuscript.

Funding
This work was supported by the National Natural Science Foundation of China (No.82460111), and Yunnan Health training project of high level talents (No. H-2024064), and the Kunming Medical University Joint Special Project on Applied Basic Research (202301AY070001-007/-210),and the Yunnan Province Famous Doctor program (YNWR-MY-2018-020), the First People's Hospital of Yunnan Province Talent Project program (No.KHYJ-2025-04-02, 2022-KHRCBZ-B03 and the Yunnan Province Clinical Medical Center for Digestive System Diseases openning program (No. 2024YNLCYXZX0250/0116).

Data availability
There were no new data generated in this study.

Declarations

Ethical approval
There is no ethical approval applicable, as this study did not involve human participants or animals.

Consent for publication
Not applicable.

Competing interests
The authors declare that they have no competing interests.

Author details
[1]Department of Gastroenterology, The First People's Hospital of Yunnan Province, Kunming 650032, China
[2]Department of Gastroenterology, Yunnan Provincince Clinical Medical Center for Digestive System Diseases, The Affiliated Hospital of Kunming University of Science and Technology, Kunming 650032, China
[3]Department of Hepatobiliary, Pancreatic and Vascular Surgery, The First People's Hospital of Kunming, The Affiliated Calmette Hospital of Kunming Medical University, Kunming 650011, China
[4]Department of Magnetic Resonance Imaging, First People's Hospital of Yunnan Province, Kunming, Yunnan 650032, China

[5]Yunnan Provincial Clinical Medical Center for Digestive System Diseases, First People's Hospital of Yunnan Province, Kunming, China

Received: 30 August 2025 / Accepted: 4 March 2026
Published online: 17 March 2026

References

1. Liu Y, He S, Wang XL, Peng W, Chen QY, Chi DM, Chen JR, Han BW, Lin GW, Li YQ, et al. Tumour heterogeneity and intercellular networks of nasopharyngeal carcinoma at single cell resolution. Nat Commun. 2021;12:741.
2. Arora R, Cao C, Kumar M, Sinha S, Chanda A, McNeil R, Samuel D, Arora RK, Matthews TW, Chandarana S, et al. Spatial transcriptomics reveals distinct and conserved tumor core and edge architectures that predict survival and targeted therapy response. Nat Commun. 2023;14:5029.
3. Cao J, Spielmann M, Qiu X, Huang X, Ibrahim DM, Hill AJ, Zhang F, Mundlos S, Christiansen L, Steemers FJ, et al. The single-cell transcriptional landscape of mammalian organogenesis. Nature. 2019;566:496–502.
4. Steen CB, Liu CL, Alizadeh AA, Newman AM. Profiling Cell Type Abundance and Expression in Bulk Tissues with CIBERSORTx. Methods Mol Biol. 2020;2117:135–57.
5. Zhou B, Bie F, Zang R, Zhang M, Song P, Liu L, Peng Y, Bai G, Huai Q, Li Y, et al. Global burden and temporal trends in incidence and mortality of oesophageal cancer. J Adv Res. 2023;50:135–44.
6. Sung H, Ferlay J, Siegel RL, Laversanne M, Soerjomataram I, Jemal A, Bray F. Global Cancer Statistics 2020: GLOBOCAN Estimates of Incidence and Mortality Worldwide for 36 Cancers in 185 Countries. CA Cancer J Clin. 2021;71:209–49.
7. Morgan E, Soerjomataram I, Rumgay H, Coleman HG, Thrift AP, Vignat J, Laversanne M, Ferlay J, Arnold M. The Global Landscape of Esophageal Squamous Cell Carcinoma and Esophageal Adenocarcinoma Incidence and Mortality in 2020 and Projections to 2040: New Estimates From GLOBOCAN 2020. Gastroenterology. 2022;163:649–e658642.
8. Wu T, Dai Y. Tumor microenvironment and therapeutic response. Cancer Lett. 2017;387:61–8.
9. The global challenge of cancer. Nat Cancer. 2020;1:1–2.
10. Chang J, Zhao X, Wang Y, Liu T, Zhong C, Lao Y, Zhang S, Liao H, Bai F, Lin D, Wu C. Genomic alterations driving precancerous to cancerous lesions in esophageal cancer development. Cancer Cell. 2023;41:2038–50. e2035.
11. Luo H, Lu J, Bai Y, Mao T, Wang J, Fan Q, Zhang Y, Zhao K, Chen Z, Gao S, et al. Effect of Camrelizumab vs Placebo Added to Chemotherapy on Survival and Progression-Free Survival in Patients With Advanced or Metastatic Esophageal Squamous Cell Carcinoma: The ESCORT-1st Randomized Clinical Trial. JAMA. 2021;326:916–25.
12. Baba Y, Yoshida N, Kinoshita K, Iwatsuki M, Yamashita YI, Chikamoto A, Watanabe M, Baba H. Clinical and Prognostic Features of Patients With Esophageal Cancer and Multiple Primary Cancers: A Retrospective Single-institution Study. Ann Surg. 2018;267:478–83.
13. Hu HF, Xu WW, Zhang WX, Yan X, Li YJ, Li B, He QY. Identification of miR-515-3p and its targets, vimentin and MMP3, as a key regulatory mechanism in esophageal cancer metastasis: functional and clinical significance. Signal Transduct Target Ther. 2020;5:271.
14. Chen L, Zhu S, Liu T, Zhao X, Xiang T, Hu X, Wu C, Lin D. Aberrant epithelial cell interaction promotes esophageal squamous-cell carcinoma development and progression. Signal Transduct Target Ther. 2023;8:453.
15. Chen Y, Zhu S, Liu T, Zhang S, Lu J, Fan W, Lin L, Xiang T, Yang J, Zhao X, et al. Epithelial cells activate fibroblasts to promote esophageal cancer development. Cancer Cell. 2023;41:903–e918908.
16. Wu H, Chen S, Yu J, Li Y, Zhang XY, Yang L, Zhang H, Hou Q, Jiang M, Brunicardi FC, et al. Single-cell Transcriptome Analyses Reveal Molecular Signals to Intrinsic and Acquired Paclitaxel Resistance in Esophageal Squamous Cancer Cells. Cancer Lett. 2018;420:156–67.
17. Patel AP, Tirosh I, Trombetta JJ, Shalek AK, Gillespie SM, Wakimoto H, Cahill DP, Nahed BV, Curry WT, Martuza RL, et al. Single-cell RNA-seq highlights intratumoral heterogeneity in primary glioblastoma. Science. 2014;344:1396–401.
18. Marx V. Method of the Year: spatially resolved transcriptomics. Nat Methods. 2021;18:9–14.
19. Tirosh I, Venteicher AS, Hebert C, Escalante LE, Patel AP, Yizhak K, Fisher JM, Rodman C, Mount C, Filbin MG, et al. Single-cell RNA-seq supports a developmental hierarchy in human oligodendroglioma. Nature. 2016;539:309–13.
20. Hao Y, Hao S, Andersen-Nissen E, Mauck WM 3rd, Zheng S, Butler A, Lee MJ, Wilk AJ, Darby C, Zager M, et al. Integrated analysis of multimodal single-cell data. Cell. 2021;184:3573–e35873529.
21. Stuart T, Butler A, Hoffman P, Hafemeister C, Papalexi E, Mauck WM 3rd, Hao Y, Stoeckius M, Smibert P, Satija R. Comprehensive Integration of Single-Cell Data. Cell. 2019;177:1888–902. e1821.
22. Robles-Remacho A, Sanchez-Martin RM, Diaz-Mochon JJ. Spatial Transcriptomics: Emerging Technologies in Tissue Gene Expression Profiling. Anal Chem. 2023;95:15450–60.
23. Lewis SM, Asselin-Labat M-L, Nguyen Q, Berthelet J, Tan X, Wimmer VC, Merino D, Rogers KL, Naik SH. Spatial omics and multiplexed imaging to explore cancer biology. Nat Methods. 2021;18:997–1012.
24. Ji AL, Rubin AJ, Thrane K, Jiang S, Reynolds DL, Meyers RM, Guo MG, George BM, Mollbrink A, Bergenstrahle J, et al. Multimodal Analysis of Composition and Spatial Architecture in Human Squamous Cell Carcinoma. Cell. 2020;182:1661–2.
25. Rao A, Barkley D, França GS, Yanai I. Exploring tissue architecture using spatial transcriptomics. Nature. 2021;596:211–20.
26. Christofori G. New signals from the invasive front. Nature. 2006;441:444–50.
27. Korsunsky I, Millard N, Fan J, Slowikowski K, Zhang F, Wei K, Baglaenko Y, Brenner M, Loh PR, Raychaudhuri S. Fast, sensitive and accurate integration of single-cell data with Harmony. Nat Methods. 2019;16:1289–96.
28. Dobin A, Davis CA, Schlesinger F, Drenkow J, Zaleski C, Jha S, Batut P, Chaisson M, Gingeras TR. STAR: ultrafast universal RNA-seq aligner. Bioinformatics. 2013;29:15–21.
29. Yu G, Wang LG, Han Y, He QY. clusterProfiler: an R package for comparing biological themes among gene clusters. Omics. 2012;16:284–7.
30. Liberzon A, Subramanian A, Pinchback R, Thorvaldsdóttir H, Tamayo P, Mesirov JP. Molecular signatures database (MSigDB) 3.0. Bioinformatics. 2011;27:1739–40.
31. Subramanian A, Tamayo P, Mootha VK, Mukherjee S, Ebert BL, Gillette MA, Paulovich A, Pomeroy SL, Golub TR, Lander ES, Mesirov JP. Gene set enrichment analysis: a knowledge-based approach for interpreting genome-wide expression profiles. Proc Natl Acad Sci U S A. 2005;102:15545–50.
32. Hänzelmann S, Castelo R, Guinney J. GSVA: gene set variation analysis for microarray and RNA-seq data. BMC Bioinformatics. 2013;14:7.
33. Browaeys R, Saelens W, Saeys Y. NicheNet: modeling intercellular communication by linking ligands to target genes. Nat Methods. 2020;17:159–62.
34. Feng LY, Huang YZ, Zhang W, Li L. LAMA3 DNA methylation and transcriptome changes associated with chemotherapy resistance in ovarian cancer. J Ovarian Res. 2021;14:67.
35. Ning B, Mei Y. LAMA3 Promotes Tumorigenesis of Oral Squamous Cell Carcinoma by METTL3-Mediated N6-Methyladenosine Modification. Crit Rev Immunol. 2024;44:49–59.
36. Bill R, Wirapati P, Messemaker M, Roh W, Zitti B, Duval F, Kiss M, Park JC, Saal TM, Hoelzl J, et al. CXCL9:SPP1 macrophage polarity identifies a network of cellular programs that control human cancers. Science. 2023;381:515–24.
37. Fu M, Shu S, Peng Z, Liu X, Chen X, Zeng Z, Yang Y, Cui H, Zhao R, Wang X, et al. Single-Cell RNA Sequencing of Coronary Perivascular Adipose Tissue From End-Stage Heart Failure Patients Identifies SPP1(+) Macrophage Subpopulation as a Target for Alleviating Fibrosis. Arterioscler Thromb Vasc Biol. 2023;43:2143–64.
38. Liu J, Huang Y, Gong Y, Liu Q, Lin J, Liu J, Liu M, Huang J, Pu W, Ma Y, et al. CTHRC1 + fibroblasts are stimulated by macrophage-secreted SPP1 to induce excessive collagen deposition in keloids. Clin Transl Med. 2022;12:e1115.
39. Qi J, Sun H, Zhang Y, Wang Z, Xun Z, Li Z, Ding X, Bao R, Hong L, Jia W, et al. Single-cell and spatial analysis reveal interaction of FAP(+) fibroblasts and SPP1(+) macrophages in colorectal cancer. Nat Commun. 2022;13:1742.
40. Morse C, Tabib T, Sembrat J, Buschur KL, Bittar HT, Valenzi E, Jiang Y, Kass DJ, Gibson K, Chen W, et al. Proliferating SPP1/MERTK-expressing macrophages in idiopathic pulmonary fibrosis. Eur Respir J. 2019;54.

Publisher's note